Effective shear and bulk viscosities for anisotropic flow

Fernando G. Gardim[1] and Jean-Yves Ollitrault[2]

[1]Instituto de Ciência e Tecnologia, Universidade Federal de Alfenas, 37715-400 Poços de Caldas, MG, Brazil
[2]Université Paris-Saclay, CNRS, CEA, Institut de physique théorique, 91191, Gif-sur-Yvette, France
(Dated: October 23, 2020)

We evaluate the viscous damping of anisotropic flow in heavy-ion collisions for arbitrary temperature-dependent shear and bulk viscosities. We show that the damping is solely determined by effective shear and bulk viscosities, which are weighted averages over the temperature. We determine the relevant weights for nucleus-nucleus collisions at $\sqrt{s_{\rm NN}} = 5.02$ TeV and 200 GeV, corresponding to the maximum LHC and RHIC energies, by running ideal and viscous hydrodynamic simulations. The effective shear viscosity is driven by temperatures below 210 MeV at RHIC, and below 280 MeV at the LHC, with the largest contributions coming from the lowest temperatures, just above freeze-out. The effective bulk viscosity is driven by somewhat higher temperatures, corresponding to earlier stages of the collision. We show that at a fixed collision energy, the effective viscosity is independent of centrality and system size, and that the variation of viscous damping is determined by Reynolds number scaling.

I. INTRODUCTION

Determining the transport coefficients of the quark-gluon plasma, such as its shear (η) and bulk (ζ) viscosities, is one of the goals of heavy-ion physics. One of the motivations is the early recognition that the quark-gluon plasma produced in heavy-ion collisions has a very low shear viscosity over entropy (η/s) ratio [1], implying the formation of a strongly-coupled fluid [2]. Shear viscosity is now included in the vast majority of state-of-the art hydrodynamic simulations of heavy-ion collisions [3]. It has been shown that bulk viscosity must also be taken into account in order to quantitatively explain experimental data [4].

Ab-initio calculations of transport coefficients with lattice techniques pose serious numerical and theoretical challenges [5]. There is nevertheless a theoretical consensus that they depend strongly on temperature [6, 7], both in the hadronic phase [8] and in the deconfined phase [9]. Over the last decade, several efforts have been made to incorporate this temperature dependence into hydrodynamic calculations [10–12]. An important question is how this temperature dependence can be constrained using experimental data [13, 14]. A recent study shows that η/s is most constrained in the temperature range $T \sim 150 - 220$ MeV [15].

The phenomenon that allows one to best constrain η/s and ζ/s is anisotropic flow [3], by which the distribution of outgoing particles breaks azimuthal symmetry. The azimuthal anisotropy, which is characterized by Fourier coefficients v_n, builds up gradually as a result of the collective expansion [16]. Viscosity makes the expansion less collective, thus reducing v_n.

We carry out a systematic investigation of this decrease for the two largest harmonics, v_2 [1] and v_3 [17]. In Sec. II, we show that the reduction in v_n due to viscosity can be written as a weighted integral of the temperature-dependent η/s and ζ/s. We define effective viscosities, which encapsulate the information on viscosity that one can gain from anisotropic flow. In Sec. III, we deter-

mine the weights that define the effective viscosities by running hydrodynamic simulations of central Pb+Pb collisions at $\sqrt{s_{\rm NN}} = 5.02$ TeV. In Sec. IV, we check that the order of magnitude of viscous damping is compatible with expectations from dimensional analysis. In Sec. V, we show that the effective viscosity is an excellent predictor of the viscous suppression of v_n for a wide range of temperature-dependent shear and bulk viscosities. In Sec. VI, we check that the centrality and system-size dependence of the viscous damping follows the $1/R$ scaling expected from dimensional analysis, where R is the transverse size. The dependence on collision energy is illustrated in Sec. VII where we carry out calculations at $\sqrt{s_{\rm NN}} = 200$ GeV, corresponding to the top RHIC energy.

II. EFFECTIVE VISCOSITY

We define effective bulk and shear viscosities of hot quark and gluon matter, which determine the damping of anisotropic flow.

A hydrodynamic simulation starts from an initial condition, corresponding typically to the entropy density profile at an early time. One then solves the equations of hydrodynamics, which model the expansion of the system into the vacuum. We study the effect of viscosity by evolving the same initial profile through ideal hydrodynamics ($\eta/s = \zeta/s = 0$) and viscous hydrodynamics. The fluid eventually fragments into individual hadrons, and we evaluate v_n from the distribution of outgoing particles in both cases. We use the following quantity as a measure of the viscous damping:

$$\Delta_n \equiv \ln \left(\frac{v_n(\text{viscous})}{v_n(\text{ideal})} \right). \tag{1}$$

If $|\Delta_n| \ll 1$, then, Δ_n is the relative change of v_n due to viscosity, $\Delta_n \simeq v_n(\text{viscous})/v_n(\text{ideal}) - 1$. One typically expects viscosity to reduce v_n [1], resulting in a negative Δ_n.

Our study is limited to v_2 and v_3 because their dependence on the initial density profile is, to a good approximation [18], a linear response to the corresponding initial anisotropy ε_n [19], both in ideal and viscous hydrodynamics, so that the dependence cancels when taking the ratio in Eq. (1). Therefore, even though we evaluate Δ_n with a specific, smooth density profile, which will be specified in Sec. III, we expect the result to be universal to a good approximation. This should however be checked explicitly when initial-state fluctuations are present [20–22]. We plan to do this in a future work.

We now derive the general expression of Δ_n in the limit of small viscosities. Δ_n is a functional of $(\eta/s)(T)$ and $(\zeta/s)(T)$, which vanishes by construction if $(\eta/s)(T) = (\zeta/s)(T) = 0$. Transport coefficients enter the equations of viscous hydrodynamics as two separate linear contributions [23] Therefore, for small $(\eta/s)(T)$ and $(\zeta/s)(T)$, Δ_n must be a linear functional of these quantities [24]:

$$\Delta_n = \int_{T_f}^{\infty} \frac{\eta}{s}(T)w_n^{(\eta)}(T)dT + \int_{T_f}^{\infty} \frac{\zeta}{s}(T)w_n^{(\zeta)}(T)dT, \quad (2)$$

where T_f is the lowest value of the temperature, called the freeze-out temperature, and $w_n^{(\eta)}(T)$ and $w_n^{(\zeta)}(T)$ are weight functions for shear and bulk viscosity. These weight functions quantify the effect of viscosity on anisotropic flow at a given temperature.

We define the effective shear and bulk viscosities relevant for v_n by:

$$\left(\frac{\eta}{s}\right)_{n,\text{eff}} = \frac{\int_{T_f}^{\infty}(\eta/s)(T)w_n^{(\eta)}(T)dT}{\int_{T_f}^{\infty}w_n^{(\eta)}(T)dT}$$
$$\left(\frac{\zeta}{s}\right)_{n,\text{eff}} = \frac{\int_{T_f}^{\infty}(\zeta/s)(T)w_n^{(\zeta)}(T)dT}{\int_{T_f}^{\infty}w_n^{(\zeta)}(T)dT}. \quad (3)$$

Then, Eq. (2) expresses the damping of v_n as

$$\Delta_n = W_n^{(\eta)} \times \left(\frac{\eta}{s}\right)_{n,\text{eff}} + W_n^{(\zeta)} \times \left(\frac{\zeta}{s}\right)_{n,\text{eff}}, \quad (4)$$

where

$$W_n^{(\eta,\zeta)} \equiv \int_{T_f}^{\infty} w_n^{(\eta,\zeta)}(T)dT. \quad (5)$$

Equation (4) implies that for any temperature-dependent viscosity, the damping of v_n is solely determined by the effective shear and bulk viscosities defined by Eq. (3). This result holds in the limit of small viscosity. Note, however, that the validity of hydrodynamics itself requires that viscosity has a small relative effect on observables, since viscous hydrodynamics is the first term in a systematic gradient expansion [25]. We therefore postulate that our result is general, and that the damping of v_n is always determined by the effective viscosities. This will be checked explicitly in Sec. V.

The effective viscosity (3) is a weighted average of the temperature-dependent viscosity. It is similar to the quantity recently introduced by Paquet *et al.* [24], but applied to different observables (anisotropic flow, as opposed to entropy), so that weights are different. We determine the relevant weights for anisotropic flow in Sec. III. We then test the validity of Eq. (4) in Sec. V.

III. DETERMINING THE WEIGHTING FUNCTIONS

In this Section, we determine the weighting functions $w_n^{(\eta)}(T)$ and $w_n^{(\zeta)}(T)$, which define the effective viscosity (3), for central Pb+Pb collisions at the top LHC energy $\sqrt{s_{\text{NN}}} = 5.02$ TeV. We carry out two separate sets of hydrodynamic simulations, one with only shear viscosity and one with only bulk viscosity. In order to isolate the effect of the viscosity in a specific temperature range, we implement a viscosity profile which is a narrow window of width σ, centered around a temperature T_0:

$$\frac{\eta}{s}(T) = \left(\frac{\eta}{s}\right)_{\text{max}} \exp\left(-\frac{(T-T_0)^2}{2\sigma^2}\right), \quad (6)$$

where $(\eta/s)_{\text{max}}$ the maximum value of η/s. We carry out simulations for a large number of values of T_0, which span the range of temperatures in a heavy-ion collision. The exact same procedure is repeated for bulk viscosity, replacing η/s with ζ/s.

The first thought would be to use a window as narrow as possible. If σ is too small, however, there are large errors for the following reason: The viscosity varies steeply with the temperature, which itself depends on space-time coordinates. This results in large pressure gradients, while they should always be small in hydrodynamics [25]. These gradients are proportional to $(\eta/s)_{\text{max}}/\sigma$. When gradients are too large, we find that instabilities occur, which appear as numerical errors (e.g., v_n jumping up and down upon small variations of T_0). We have adjusted the values of parameters so that results are stable. Our simulations are carried out with $\sigma = 16$ MeV, $(\eta/s)_{\text{max}} = 0.04$ (Fig. 1 (a)) and $(\zeta/s)_{\text{max}} = 0.02$ (Fig. 1 (b)).

Our hydrodynamic simulation uses boost-invariant [26] initial conditions, with a starting time $\tau_0 = 0.6$ fm/c. The transverse velocity at τ_0 is set to zero, that is, initial flow [27, 28] is neglected. The initial entropy density profile is a deformed Gaussian [17]:

$$s(x,y) = s(r\cos\phi, r\sin\phi)$$
$$= s_0 \exp\left(-\frac{r^2}{R_0^2}\left(1 + \varepsilon_2\cos 2\phi + \frac{4}{5}\varepsilon_3\cos 3\phi\right)\right) (7)$$

In this equation, ε_2 and ε_3 are the initial eccentricities [29],[1] which produce elliptic flow and triangular flow after hydrodynamic expansion.

————

[1] ε_2 and ε_3 in Eq. (7) correspond to the usual eccentricities [30] only in the limit where they are much smaller than unity, more precisely, to first order in ε_2 and ε_3.
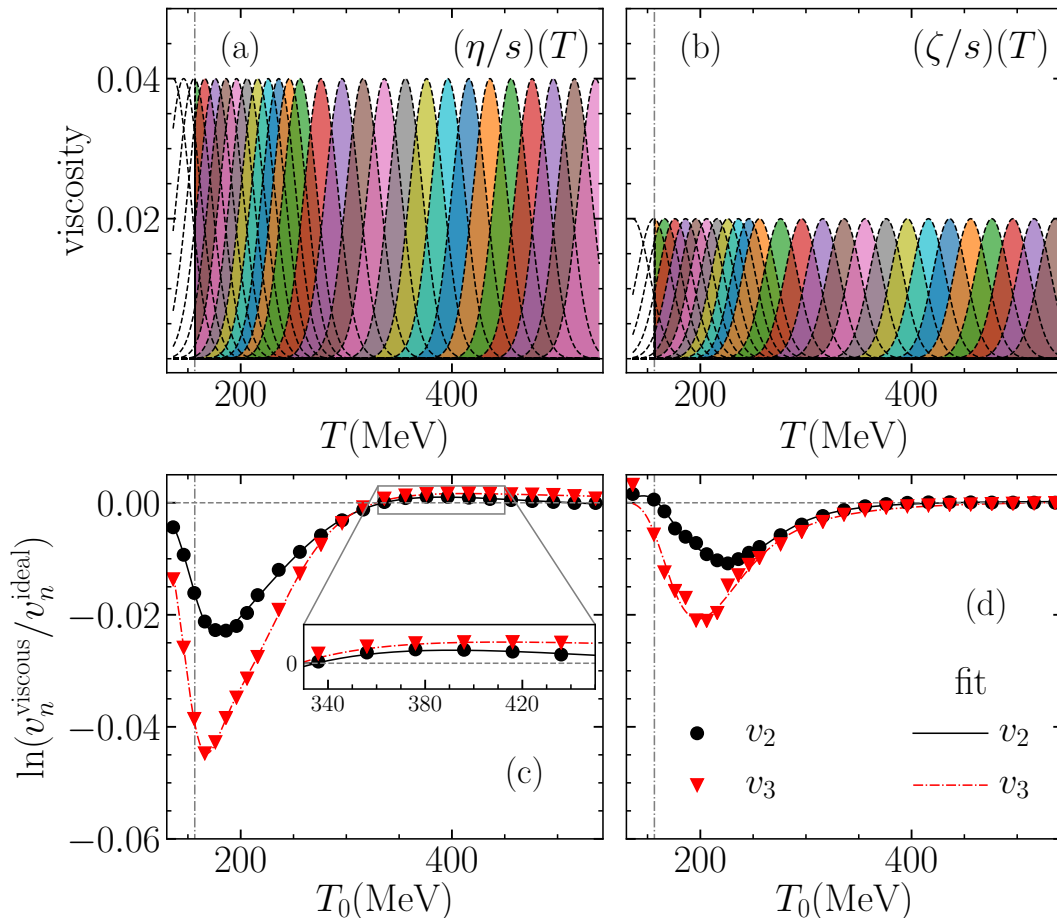
FIG. 1. (Color online) Effect of a temperature-dependent shear (η) or bulk (ζ) viscosity on v_2 and v_3 in central Pb+Pb collisions at $\sqrt{s_{NN}} = 5.02$ TeV. Shear corresponds to the left panels (a) and (c), bulk to the right panels (b) and (d). The upper panels dispay the (η/s) and (ζ/s) profiles used in our caculation. They are defined by Eq. (6), with $\sigma = 16$ MeV, $(\eta/s)_{\max} = 0.04$ (a) and $(\zeta/s)_{\max} = 0.02$ (b), and each curve corresponds to a different value of T_0. The vertical lines indicate the freeze-out temperature $T_f = 156.5$ MeV. The symbols in panels (c) and (d) display the corresponding values of Δ_n, defined by Eq. (1), as a function of T_0. Lines are fits using Eqs. (2) and (8).

We fix the parameters of Eq. (7) as follows: We evaluate R_0 by matching the rms radius to a model of initial conditions that reproduces well the mean transverse momentum $\langle p_t \rangle$ [31], since $\langle p_t \rangle$ is determined by the initial radius in hydrodynamics [32, 33]. We then fix the normalization constant s_0 in such a way that the multiplicity matches that measured in Pb+Pb collisions at $\sqrt{s_{NN}} = 5.02$ TeV [34]. Since the multiplicity is proportional to the final entropy, which is larger than the initial entropy in viscous hydrodynamics [35], the normalization s_0 must be lowered in viscous hydrodynamics.[2]

Finally, we evaluate ε_2 and ε_3 from a model of initial conditions [36] which reproduces well the measured values of v_2 and v_3.[3] The resulting density profile is represented in Fig. 2 (a) for central collisions.

We then evolve this initial condition using the MUSIC hydrodynamic code [37–39] with a realistic equation of state inspired by lattice QCD [40]. We evaluate v_2 and v_3 at the freeze-out temperature $T_f = 156.5$ MeV [41]. The viscous corrections to the momentum distribution at freeze out are evaluated using the usual quadratic ansatz [42, 43]. We take into account hadronic decays, but we neglect rescatterings in the hadronic phase. For the sake of simplicity, we evaluate v_2 and v_3 (averaged

---

[2] In practice, we choose s_0 for viscous hydrodynamics so that the final multiplicity is close to the expected value. We then evaluate v_n in ideal hydrodynamics for the corresponding final multiplicity by linear interpolation between calculations run with two different values of s_0.

---

[3] This is not crucial as our final results are independent of ε_2 and ε_3.
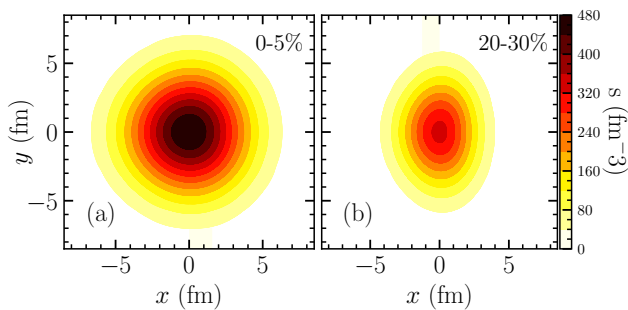
FIG. 2. (Color online) Initial entropy density profile used in our ideal hydrodynamic calculation, defined by Eq. (7), with parameters tuned to match Pb+Pb collisions at $\sqrt{s_{\rm NN}} =$ 5.02 TeV. (a) 0-5% centrality window (Secs. III—V): $s_0 =$ 438 fm^{-3}, $R_0 = 4.18$ fm, $\varepsilon_2 = 0.085$, $\varepsilon_3 = 0.075$. (b) 20-30% centrality window (Sec. VI): $s_0 = 337$ fm^{-3}, $R_0 = 2.97$ fm, $\varepsilon_2 = 0.35$, $\varepsilon_3 = 0.12$. The profile is identical for the viscous hydrodynamic calculation, except for the overall normalization (see text).

over all transverse momenta p_t), in the same pseudorapidity window $|\eta| < 0.5$ used to measure the multiplicity [34]. The fact that experiments use different pseudorapidity cuts [44] matters little, since these kinematic cuts typically multiply v_n by a constant factor, which cancels when evaluating Δ_n using Eq. (1).
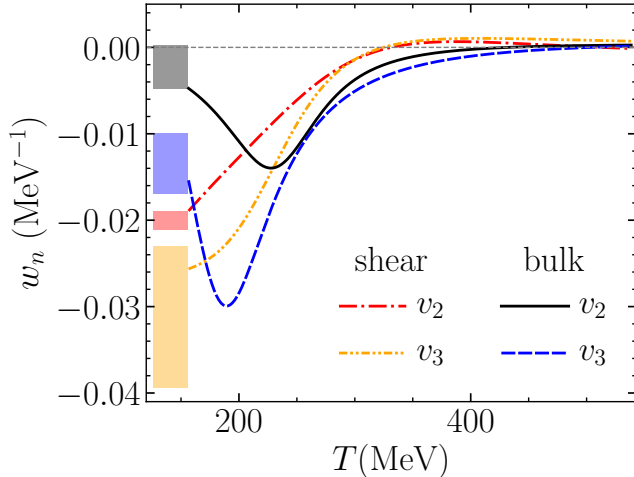

FIG. 3. (Color online) Weights $w_2^\zeta(T)$ (full line), $w_3^\zeta(T)$ (dashed line), $w_2^\eta(T)$ (dot-dashed line), $w_3^\eta(T)$ (dotted line), defining the effective viscosities (3) at $\sqrt{s_{\rm NN}} = 5.02$ TeV. They are obtained by fitting the hydrodynamic results in Fig. 1 using Eq. (8). The shaded boxes to the left are meant to represent the discrete part $w_f \delta(T - T_f)$: Their area is $|w_f|$ (see numbers in Table I).

The values of Δ_n are displayed in Fig. 1 (c) and (d) for shear and bulk viscosity, as a function of the temperature T_0 in Eq. (6). Δ_n is mostly negative, which means

that viscosity decreases anisotropic flow [1]. Δ_2 and Δ_3 have similar variations as a function of T_0, but the overall magnitude of Δ_3 is larger, both for shear and bulk viscosity: As expected, damping is stronger for higher harmonics [17, 45]. Large negative values of Δ_n are obtained for values of T_0 around 200 MeV, corresponding to the late stages of the hydrodynamic evolution. For $T_0 > 300$ MeV, corresponding to a viscosity which is only present during the early stages, Δ_n is much smaller. Interestingly, for shear viscosity, Δ_n changes sign and becomes positive for $T_0 > 330$ MeV (see the zoom in Fig. 1 (c)). This implies that shear viscosity at high temperature *increases* v_n, although by a very modest amount. The physical interpretation is that when the longitudinal expansion dominates, shear viscosity reduces the longitudinal pressure and increases the transverse pressure, leading to an increased transverse flow in general, and anisotropic flow in particular.

Using the results for Δ_n, we then infer $w_n^{(\eta,\zeta)}(T)$ defined by Eq. (2). One would naively expect $w_n^{(\eta,\zeta)}(T)$ to be a smooth function of T. However, one must remember that viscosity enters a hydrodynamic simulation in two different places: (1) In the equations of hydrodynamics themselves; (2) At the final stage when the fluid is transformed into particles. The effect of viscosity on the hydrodynamic flow [46] builds up throughout the expansion, and one expects the resulting contribution to $w_n^{(\eta,\zeta)}(T)$ to be smooth. On the other hand, the viscous correction to the momentum distribution at freezeout [42, 43, 47] only involves the viscosity at T_f. Therefore, we decompose $w_n^{(\eta,\zeta)}(T)$ as the sum of a smooth function, which we approximate by a rational function (Padé approximant), and a discrete contribution in the form of a Dirac peak at T_f:

$$w(T) = w_f \delta(T - T_f) + \frac{a_0 + a_1 T + a_2 T^2}{1 + b_1 T + b_2 T^2 + b_3 T^3} \quad (8)$$

where we have used the shortcut $w(T)$ for $w_n^{(\eta,\zeta)}(T)$. The parameters w_f, a_i and b_i are fitted to the Δ_n results using Eq. (2). The fits are shown as lines in panels (c) and (d) of Fig. 1. In order to better constrain the relative magnitudes of the discrete and the smooth contributions, we have carried out a few simulations where T_0 is lower than the freeze-out temperature T_f (see Fig. 1 (a) and (b)). In these simulations, the discrete term dominates the viscous correction.

The smooth parts of the weighting functions $w_n^{(\eta,\zeta)}(T)$ are displayed in Fig. 3.[4] For shear viscosity, the lowest values of T get the largest weights in absolute value. This

————

[4] Note that the variation of $w_n^{(\eta,\zeta)}(T)$ as a function of T follows that of Δ_n in Fig. 1 as a function of T_0, except for the values of T_0 close to the freeze-out temperature. This can be understood easily: In the limit where $T_0 - T_f \gg \sigma$, inserting Eq. (6) into Eq. (2) and assuming that $w_n^{(\eta,\zeta)}(T)$ varies little over a temperature

	n	w_f	$W \equiv \int_{T_f^-} w(T)dT$
shear	2	-0.07	-1.34
bulk	2	0.15	-1.30
shear	3	-0.49	-2.33
bulk	3	0.21	-2.61

TABLE I. Values of w_f (Eq. (8)) and W (Eq. (5)) for elliptic ($n = 2$) and triangular ($n = 3$) flows, and for shear and bulk viscosity, in central Pb+Pb collisions at $\sqrt{s_{\rm NN}} = 5.02$ TeV.

explains the conclusion from a recent Bayesian study that η/s is best constrained in the range $150 < T < 220$ MeV [15]. For bulk viscosity, on the other hand, the weight has a peak for intermediate values of the temperature, around 230 MeV for v_2, and 190 MeV for v_3. The discrete part w_f of the viscous correction, corresponding to the first term in Eq. (8), is given in Table I. It originates from the viscous correction to the thermal momentum distribution [42]. This correction depends on the microscopic dynamics at freeze-out [47], which is not well understood. By constrast, the smooth part of Eq. (8), which is the viscous correction that builds up during the hydrodynamic evolution, solely involves the equations of hydrodynamics and is more robust. Looking at the numbers in Table I, one sees that w_f is a small fraction of the integral W, which implies that freeze-out only accounts for a small fraction of the viscous suppression: 5% for v_2, 21% for v_3, in the case of a constant η/s. Note also that the bulk viscosity gives a small but *positive* contribution to v_n at freeze-out.[5] The fact that w_f is small guarantees that the determination of Δ_n in viscous hydrodynamics is fairly robust with respect to model uncertainties. Note that this is because we have evaluated the p_t-integrated v_n, which is largely determined by the energy-momentum tensor. In a specific p_t range, the dependence on the momentum distribution would typically be larger. As we shall see in Sec. VII, w_f represent a much larger fraction of the viscous correction at lower energies.

---

range of order σ, one can approximate $w_n^{(\eta,\zeta)}(T) \simeq w_n^{(\eta,\zeta)}(T_0)$, and one obtains:

$$w_n^{(\eta)}(T_0) \simeq \frac{\Delta_n(T_0)}{(\eta/s)_{\rm max}\sigma\sqrt{2\pi}}, \qquad (9)$$

and a similar formula for bulk viscosity. For temperatures close to the freeze-out temperature $T_f = 156.5$ MeV, there are differences between the variations of Δ_n and w_n, which are apparent in particular for shear viscosity, where the leftmost point for $\Delta_{2,3}$ goes up, while the variation of $w_{2,3}^{(\eta)}(T)$ is monotonic down to T_f. The reason is that for these values of T_0, part of the Gaussian profile is cut at T_f (see Fig. 1 (a) and (b)), resulting in a smaller value of Δ_n.

[5] This can be inferred from the observation that $\Delta_n > 0$ for $T_0 < T_f$ in Fig. 1 (d).

IV. ORDERS OF MAGNITUDE AND DIMENSIONAL ANALYSIS

Before we embark on quantitative tests of the "effective viscosity" approach, we analyze the order of magnitude of the viscous suppression. For a constant shear viscosity over entropy ratio $\eta/s = 0.08$ [2], Eq. (4) together with the numerical values in Table I gives $\Delta_2 = -0.11$ and $\Delta_3 = -0.19$, corresponding to 10% and 17% reductions in v_2 and v_3, respectively, according to Eq. (1).

We now check that these numbers are compatible with expectations from dimensional analysis. The inverse Reynolds number Re^{-1} governs the magnitude of viscous effects. It is defined as the ratio of the viscous force, which is $\eta\Delta v$ for shear viscosity, to the inertia, which is $(\epsilon + P)dv/dt$ for a relativistic fluid. Assuming that space-time derivatives are of order $1/R$, where R is the rms radius of the initial density profile, and using $\epsilon + P = Ts$, one obtains:

$$\mathrm{Re}^{-1} = \frac{(\eta/s)}{TR}. \qquad (10)$$

In this equation, is it natural to replace (η/s) by the effective viscosity $(\eta/s)_{\rm eff}$. T should be a typical temperature at which viscous effects operate, that is $T \sim 200$ MeV.

In the specific case of anisotropic flow, one can guess the order of magnitude of Δ_n with the guidance of exact solutions [49], which give an extra factor of n^2 [45]. The dimensional analysis is the same for bulk viscosity. Hence, the back-of-the-envelope estimate of Δ_n is

$$\Delta_n \sim -n^2\frac{(\eta/s)_{\rm eff} + (\zeta/s)_{\rm eff}}{TR}. \qquad (11)$$

Comparing with Eq. (4), the expected order of magnitude of the prefactor $W_n^{(\eta,\zeta)}$ is:

$$W_n^{(\eta,\zeta)} \sim -n^2\frac{1}{TR}. \qquad (12)$$

With the value $R \simeq 4.2$ fm of our initial condition (Fig. 2 (a)) and $T \sim 200$ MeV$\simeq 1$ fm^{-1}, Eq. (12) gives $W_2^{(\eta)} \sim W_2^{(\zeta)} \sim -1.0$ and $W_3^{(\eta)} \sim W_3^{(\zeta)} \sim -2.1$. The numerical values in Table I are of the expected order of magnitude. In particular, they confirm the expectation that shear and bulk viscosity have similar effects, and that the damping is stronger by a factor ~ 2 for v_3 than for v_2.

V. EFFECTIVE VISCOSITY AS A PREDICTOR OF THE DAMPING OF v_n

We now test the hypothesis that the effective viscosities (3) are good predictors of the viscous suppression Δ_n. Using the weights $w_n^{(\eta,\zeta)}(T)$ determined in Sec. III, we can evaluate the effective shear and bulk viscosities for any temperature-dependent viscosity, and then predict
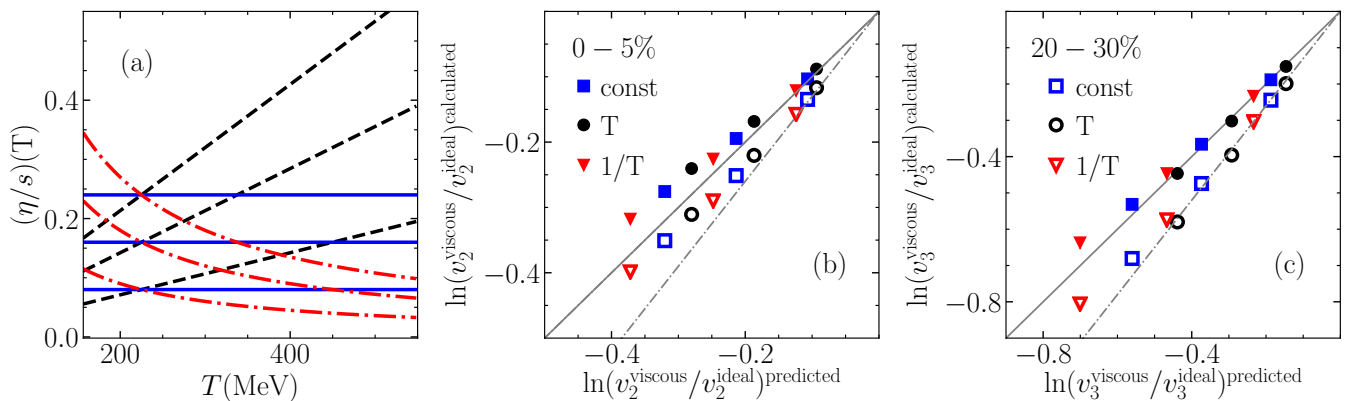
FIG. 4. (Color online) (a) Various $(\eta/s)(T)$ profiles which are used to test Eq. (2). They are defined by $(\eta/s)(T) = C$ (full lines), $(\eta/s)(T) = CT/T_0$ (dashed lines) or $(\eta/s)(T) = CT_0/T$, with $T_0 = 225$ MeV, and $C = 0.08$, 0.16, or 0.24. Panels (b) and (c) display Δ_n defined by Eq. (1), as a function of Δ_n defined by Eq. (4). Each symbol in panels (b) and (c) corresponds to one of the profiles in panel (a). Full symbols correspond to the $0 - 5\%$ centrality window (Sec. V) and open symbols correspond to the $20 - 30\%$ centrality window (Sec. VI). The full lines in panels (b) and (c) are the diagonals $y = x$, while the dash-dotted lines represent the prediction for $20 - 30\%$ centrality from Reynolds number scaling, $y = 1.32\,x$ (see text).
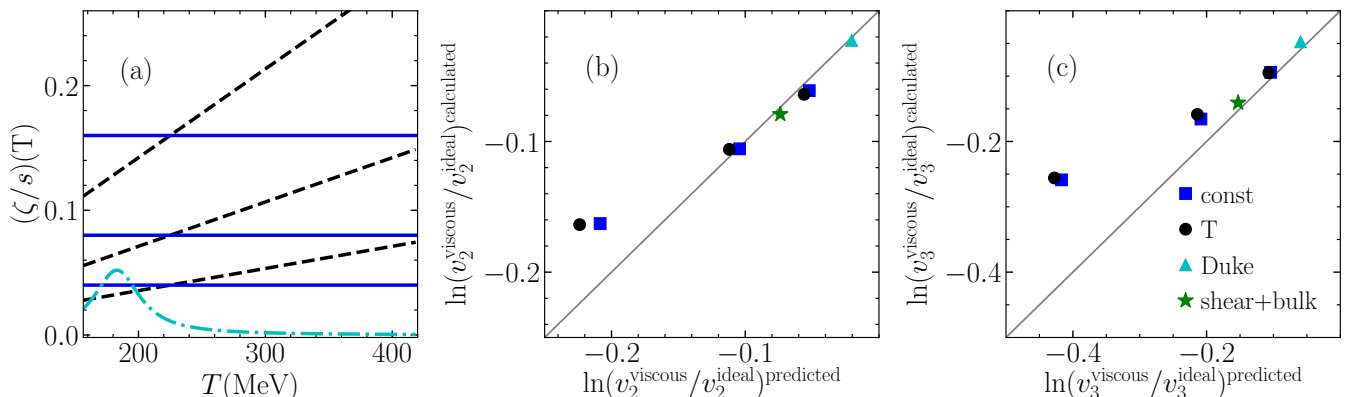

FIG. 5. (Color online) Same as Fig. 4 for bulk viscosity alone, and shear+bulk. The $(\zeta/s)(T)$ profiles are represented in panel (a). They are defined by $(\zeta/s)(T) = C$ (full lines), $(\zeta/s)(T) = CT/T_0$ (dashed lines), with $T_0 = 225$ MeV, and $C = 0.04$, 0.08, or 0.16. The dash-dotted line is the Duke parametrization [48]. Squares, circles and triangles in panels (b) and (c) correspond to the profiles in panel (a). The stars represent a calculation done with a constant shear viscosity over entropy $\eta/s = 0.04$, on top of the Duke parametrization of bulk viscosity.

the value of the viscous damping Δ_n using Eq. (4). In order to check the validity of this prediction, we carry out viscous hydrodynamic simulations with nine different $(\eta/s)(T)$ profiles, which are represented in Fig. 4 (a), and seven different $(\zeta/s)(T)$ profiles, which are represented in Fig. 5 (a). These profiles span a wide range of possibilities concerning the variation and magnitude of η/s and ζ/s.

For each of these profiles, panels (b) and (c) of Figs. 4 and 5 display the value of Δ_2 and Δ_3 computed numerically in viscous hydrodynamics using Eq. (1), as a function of the value predicted using Eq. (4). When only bulk or shear viscosity is present, the quantity on the x axis is the effective viscosity $(\eta/s)_{n,\mathrm{eff}}$ (Fig. 4) or $(\zeta/s)_{n,\mathrm{eff}}$ (Fig. 5), multiplied by the corresponding con-

stant $W_n^{(\eta,\zeta)}$. Note that the effective viscosity is not strictly identical for $n = 2$ and $n = 3$, because the weights for $n = 2$ and $n = 3$ in Fig. 3 are not exactly proportional to each other. However, they differ only by a few percent in practice.

For small $|\Delta_n|$, the calculated value agrees with the predicted value in all cases: With only shear viscosity (full symbols in Fig. 4), only bulk viscosity (full squares and circles in Fig. 5), or with shear and bulk viscosity simultaneously (stars in Fig. 5). This means that Eq. (2) holds in the limit of small viscosity, which is precisely the assumption under which it was derived. In particular, our calculation shows explicitly that shear viscosity and bulk viscosity give additive contributions to the damping

of v_n.

For larger values of $|\Delta_n|$, corresponding to larger values of η/s, the calculated values (full symbols) start to deviate from the predicted values (full lines). They are above, which implies that the dependence of v_n on $(\eta/s)_{n,\text{eff}}$ or $(\zeta/s)_{n,\text{eff}}$ is slower than exponential. These nonlinearities are stronger for bulk viscosity than for shear viscosity. Despite these deviations, all full symbols lie on the same curve. This means that the effective viscosity is an excellent predictor of Δ_n, even when viscosity suppresses v_n by a factor 2.

We now discuss the compatibility of our results with those of Niemi *et al.* [13]. They have carried out extensive simulations with different $\eta/s(T)$ profiles, which have been chosen in such a way that they yields similar v_2 and v_3. We therefore expect that these profiles correspond to similar effective viscosities. Since, furthermore, one of the profiles is a constant $\eta/s = 0.2$, we expect that $(\eta/s)_{n,\text{eff}} \sim 0.2$ for all the other profiles, both for $n = 2$ and $n = 3$. The authors provide the parameterization for three of these profiles, which are named "param1", "param2" and "param4". Comparison with our results is not straightforward because they implement partial chemical equilibrium (PCE), and run hydrodynamics down to $T_f = 100$ MeV. The energy density at $T = 100$ MeV with PCE is approximately the same as at $T = 140$ MeV without PCE. We try to take this difference into account, at least approximately, by evaluating the effective viscosity (3) with a lower value $T_f = 140$ MeV. For this purpose, we extrapolate the weights $w_n^{(\eta)}$ down to 140 MeV using Eq. (8), and we neglect the discrete contribution, which is small but depends on T_f, since we have not evaluated w_f for $T_f = 140$ MeV. We obtain $(\eta/s)_{2,\text{eff}} = 0.175$ and $(\eta/s)_{3,\text{eff}} = 0.163$ for "param1", 0.184 and 0.185 for "param2", and 0.206 and 0.207 for "param4". As expected, all effective viscosities are close to 0.2. The ordering explains the fine splitting observed in Fig. 14 (a) of Ref. [13], which shows that the damping is weakest for the "param1" parametrization, and strongest for the "param4" parametrization.

VI. CENTRALITY AND SYSTEM-SIZE DEPENDENCE

We show that at a given collision energy, the dependence of Δ_n on nuclear size and collision centrality is determined by the $1/R$ dependence expected from Reynolds number scaling, Eq. (11), and that the effective viscosity is unchanged. We first present the general argument, then the numerical results that support it.

The key observation is that the mean transverse momentum of outgoing hadrons, $\langle p_t \rangle$, is almost independent of centrality and system size: Specifically, $\langle p_t \rangle$ varies by less than 1% between 0 and 30% centrality in Pb+Pb collisions at 5.02 TeV [50], while the multiplicity decreases by a factor ~ 3 [34]. $\langle p_t \rangle$ also differs by less than 2% in Pb+Pb and Xe+Xe collisions [50], while the multiplicity

changes by a factor ~ 1.6.

In ideal hydrodynamics, the mean transverse momentum is unchanged under a uniform scaling of space-time coordinates, where the entropy density s and the fluid velocity u^ν are unchanged:

$$
\begin{aligned}
x^\mu &\to \lambda x^\mu \\
s(x^\mu) &\to s(\lambda x^\mu) \\
u^\nu(x^\mu) &\to u^\nu(\lambda x^\mu)
\end{aligned}
\tag{13}
$$

The volume and the final multiplicity, which are extensive quantities, are multiplied by λ^3, but $\langle p_t \rangle$, which is an intensive quantity, remains the same. Reversing the argument, the observation that the mean transverse momentum remain constant as one varies centrality or system size implies that these variations amount, to a good approximation, to a uniform scaling [51]. A less central collision, or a smaller nucleus, goes along with a faster expansion, but with the same density and temperature. This statement may seem counter intuitive, as one would think that more central collisions or larger nuclei imply a higher density. However, one typically has in mind a comparison at the same time, while the time coordinate should also be rescaled in Eq. (13): One should evaluate the density at an earlier time for the smaller system. A uniform scaling does not change the fraction of the space-time history that the system spends at a given temperature. Therefore, the effective viscosity, which represents the relative weights of the different temperatures, is unchanged.

The observation that the density is essentially constant as a function of centrality or system size is supported by the following theoretical argument: The multiplicity is approximately proportional to the number of constituent quarks [52], which is also proportional to the volume since the nuclear density is approximately constant. Hence the ratio multiplicity/volume does not vary significantly. Note that the shape changes as a function of the collision centrality (see Fig. 2), so that the scaling is not strictly isotropic. The anisotropy is responsible for anisotropic flow, but has a small effect on the mean transverse momentum.

We simulate mid-central collisions by adjusting the parameters of the initial density profile (7) in our hydrodynamic calculation (Fig. 2 (b)). Note that we keep the same value of the initial time ($\tau_0 = 0.6$ fm/c) for both centralities, while it should also be rescaled for the transformation (13) to be exact. However, this breaking of scale invariance occurs long before v_n develops, and we will see that it has no effect on the final results. In order to ensure that $\langle p_t \rangle$ is the same for both centralities, we require that, at a time proportional to the the rms radius R, the entropy density is the same. We therefore choose s_0 in such a way that $s_0 \tau_0 / R$ is unchanged. s_0 and R_0 are finally fixed by requesting that the final multiplicity matches the experimental value, which yields the profile

	n	w_f	$W \equiv \int_{T_f^-} w(T) dT$
shear	2	-0.67	-1.56
bulk	2	1.12	-2.33
shear	3	-2.12	-3.40
bulk	3	3.34	-3.81

TABLE II. Same as Table I for $\sqrt{s_{\mathrm{NN}}} = 200$ GeV.

in Fig. 2 (b).[6]

We then evaluate the viscous suppression of v_n in the 20-30% centrality range for the same temperature-dependent shear viscosities as in Sec. V. Results are displayed in Fig. 4 as open symbols. We plot the value of Δ_n calculated numerically with (1), as a function of the value calculated for central collisions. Therefore, closed and open symbols, corresponding to central and mid-central collisions, are vertically aligned. The open symbols are below the closed symbols, which means that the viscous suppression is larger for mid-central than for central collisions. The dot-dashed lines represent the prediction from dimensional analysis, that Δ_n is proportional to $1/R$ (Eq. (11)), implying a uniform increase by a factor 1.32. For small Δ_n, the open symbols are in excellent agreement with this prediction. They deviate from the prediction for larger $|\Delta_n|$, but they all fall on the same curve. This means that the effective shear viscosity determined in central collisions, which is the quantity on the x axis (up to a multiplicative constant) is still an excellent predictor of v_n in mid-central collisions.

The explicit calculation above is only done for shear viscosity, for one collision system and one centrality range, but conclusions are general. As long as $\langle p_t \rangle$ does not vary, the effective viscosity should remain the same. The decrease of $\langle p_t \rangle$ becomes significant for peripheral collisions, but this is also the place where the hydrodynamic description is less reliable.

VII. EFFECTIVE VISCOSITIES AT RHIC

While the effective viscosity is roughly independent of system size and centrality, it depends on the collision energy. The lower the collision energy, the lower the temperature of the quark-gluon matter formed in the collision [51], and one expects this change to reflect on the weights $w_n^{(\eta,\zeta)}(T)$ entering the effective viscosities (3). In order to illustrate this dependence on collision energy, we carry out simulations at the top RHIC energy $\sqrt{s_{\mathrm{NN}}} = 200$ GeV. We single out the dependence on collision energy by changing only the normalization constant s_0 in the initial density profile (7), and keeping all

---

[6] Due to the anisotropies, the rms radius R does not coincide with the parameter R_0 in Eq. (7). For the profile in Fig. 2 (b), for instance, $R_0 = 2.97$ fm, while $R = 3.19$ fm.

other parameters (R, ε_2, ε_3) constant. For ideal hydrodynamics, we choose $s_0 = 173$ fm^{-3}, which ensures that the charged multiplicity per nucleon matches the value measured in central Au+Au collisions [53].

The calculation is done exactly as in Sec. III. Fig. 6 is the equivalent of Fig. 1, but at the lower energy, where the temperature is $\sim 25\%$ smaller. Results for Δ_n are comparable, except for the overall temperature scale, and the overall magnitude. In particular, the small increase of v_n due to shear viscosity, which was observed for $T_0 > 330$ MeV in Fig. 1 (c), is now observed for $T_0 > 250$ MeV (see the zoom in Fig. 6 (c)).

The Δ_n results are then fitted using Eqs. (2) and (8). The integral of the weights $W_n^{(\eta,\zeta)}$, which determine the damping for a given effective viscosity according to Eq. (4), are larger at RHIC (Table II) than at the LHC (Table I). This implies that for a given effective viscosity, the damping is somewhat stronger at RHIC than at LHC. This increase is a natural consequence of the lower temperature, as shown by the estimate (12) from dimensional analysis.

The main difference with LHC energies is that the discrete contribution w_f, corresponding to the viscous correction at freeze out, is now a sizable fraction of the total W (Table II). Since, as pointed out in Sec. III, there is a theoretical uncertainty on w_f, it implies that the determination of the effective viscosity is less robust at RHIC than at the LHC.

The smooth part of the weights, displayed in Fig. 7, differs significantly from the result at the higher energy (Fig. 3), in particular for bulk viscosity. This is somewhat surprising as the results in Fig. 6, from which they are obtained, are similar to the results in Fig. 1, from which Fig. 3 is obtained. The difference is likely due to the separation between the discrete and the smooth contribution. In particular, the large negative value of $w_3^{(\zeta)}$ just above the freeze-out temperature partially compensates the effect of the large positive contribution *at* freeze out.

VIII. CONCLUSIONS

Within the hydrodynamic description of heavy-ion collisions, we have evaluated the dependence of elliptic and triangular flows on shear and bulk viscosities, for an arbitrary temperature dependence of these transport coefficients. We have assumed that v_2 and v_3 are determined by linear response to the initial anisotropies ε_2 and ε_3, and studied the dependence of the response on viscosity, thereby generalizing the study of Teaney and Yan [45], which was done for a constant η/s. We have shown that the damping is the sum of contributions from shear and bulk viscosity. Each of these contributions is determined by effective shear and bulk viscosities, which are weighted averages of the temperature-dependent viscosities.

The effective viscosities consist of a discrete part, proportional to the viscosity at freeze out, and a contin-
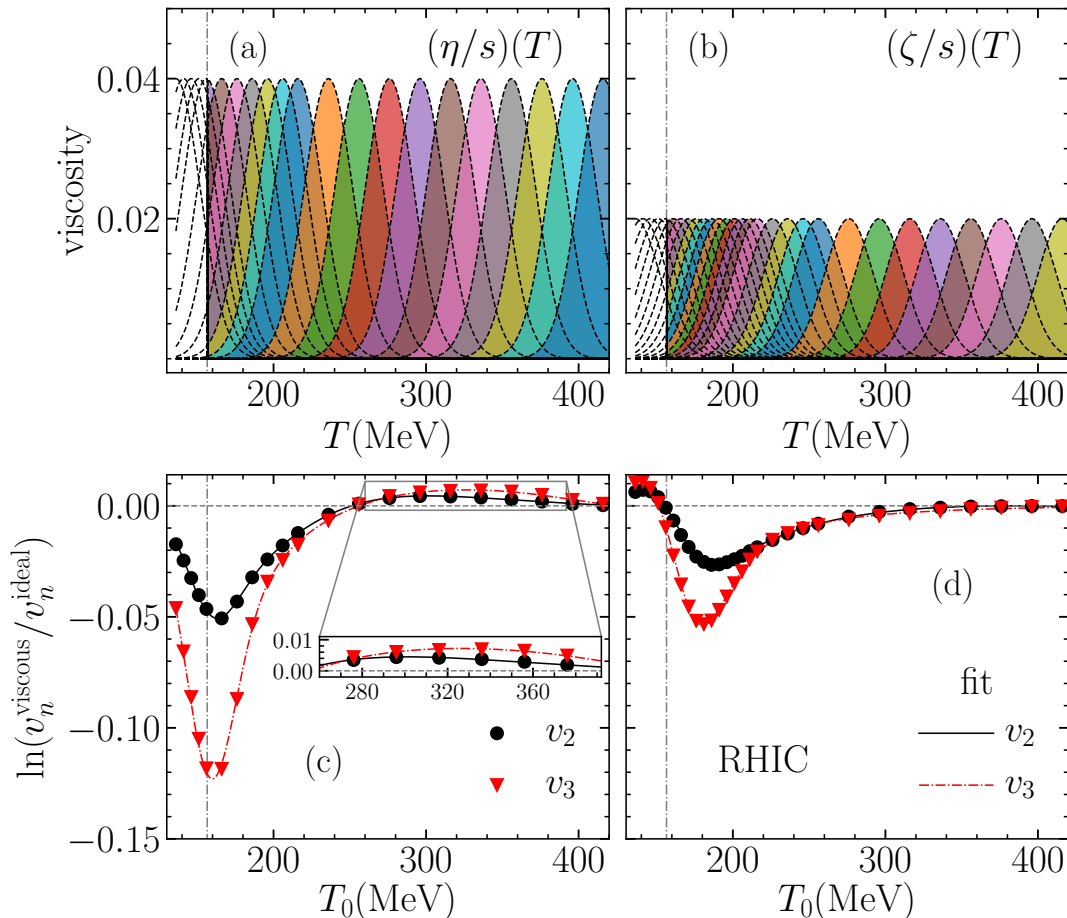
FIG. 6. (Color online) Same as Fig. 1, for the collision energy $\sqrt{s_{\mathrm{NN}}} = 200$ GeV.

uous part, which is a weighted integral of the viscosity over temperatures above the freeze-out temperature. The discrete part originates from the off-equilibrium correction to the momentum distribution of outgoing particles, while the continuous part is due to the hydrodynamic expansion itself. The discrete part is a small contribution at LHC energies. This guarantees that the determination of v_n in viscous hydrodynamics is robust with respect to uncertainties on the theoretical description of the hadronic phase. At RHIC energies, on the other hand, the discrete and the continuous contributions to the effective viscosities are of the same order of magnitude, which entails a large theoretical uncertainty.

The weights defining the effective viscosities are displayed in Figs. 3 and 7. Shear viscosity matters in the range $T < 280$ MeV at the LHC, $T < 210$ MeV at RHIC. For bulk viscosity, the weights decrease less quickly, so that higher temperatures, corresponding to earlier stages of the expansion, are comparatively more important. Interestingly, shear viscosity at early times, corresponding to the largest temperatures, results in a small *increase* of anisotropic flow.

We have shown that the effective viscosity is independent of centrality and system size at a given collision energy. The dependence of the damping on centrality and system size follows the $1/R$ dependence expected on the basis of Reynolds number scaling, where R is the transverse radius. Furthermore, effective viscosities are very similar for v_2 and v_3, which implies that a combined analysis of all existing v_2 and v_3 data at a given energy can at best constrain two numbers: the effective shear and bulk viscosities at this energy. This in turn implies that the temperature dependence of transport coefficients cannot be extracted from LHC data alone, and claims from early Bayesian analyses [14] must be revisited carefully [54].[7] Bayesian analyses should be more efficient if they make use of the observation that data at a given energy only give access to the effective viscosity at that energy. Detailed information about the temperature dependence of

---

[7] Note that the extraction of the effective viscosity from data relies crucially also involves the detailed modeling of initial conditions [55, 56], which is beyond the scope of the present work.
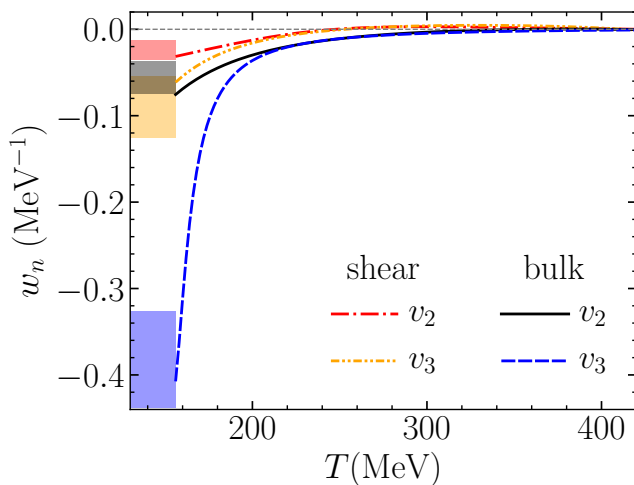
FIG. 7. (Color online) Same as Fig. 3 for $\sqrt{s_{\rm NN}} = 200$ GeV.

transport coefficients can only be obtained by a simultaneous fit to RHIC and LHC data, as recognized by the recent analysis of the JETSCAPE collaboration [57]. If, for instance, the shear viscosity over entropy ratio was large only above 200 MeV, damping of anisotropic flow would be larger at the LHC than at RHIC.

[1] P. Romatschke and U. Romatschke, Phys. Rev. Lett. **99**, 172301 (2007) doi:10.1103/PhysRevLett.99.172301 [arXiv:0706.1522 [nucl-th]].

[2] P. Kovtun, D. T. Son and A. O. Starinets, Phys. Rev. Lett. **94**, 111601 (2005) doi:10.1103/PhysRevLett.94.111601 [hep-th/0405231].

[3] U. Heinz and R. Snellings, Ann. Rev. Nucl. Part. Sci. **63**, 123 (2013) doi:10.1146/annurev-nucl-102212-170540 [arXiv:1301.2826 [nucl-th]].

[4] S. Ryu, J.-F. Paquet, C. Shen, G. S. Denicol, B. Schenke, S. Jeon and C. Gale, Phys. Rev. Lett. **115**, no. 13, 132301 (2015) doi:10.1103/PhysRevLett.115.132301 [arXiv:1502.01675 [nucl-th]].

[5] A. Bazavov *et al.* [USQCD Collaboration], Eur. Phys. J. A **55**, no. 11, 194 (2019) doi:10.1140/epja/i2019-12922-0 [arXiv:1904.09951 [hep-lat]].

[6] L. P. Csernai, J. I. Kapusta and L. D. McLerran, Phys. Rev. Lett. **97**, 152303 (2006) doi:10.1103/PhysRevLett.97.152303 [nucl-th/0604032].

[7] D. Kharzeev and K. Tuchin, JHEP **0809**, 093 (2008) doi:10.1088/1126-6708/2008/09/093 [arXiv:0705.4280 [hep-ph]].

[8] J. Noronha-Hostler, J. Noronha and C. Greiner, Phys. Rev. Lett. **103**, 172302 (2009) doi:10.1103/PhysRevLett.103.172302 [arXiv:0811.1571 [nucl-th]].

[9] J. Ghiglieri, G. D. Moore and D. Teaney, JHEP **1803**, 179 (2018) doi:10.1007/JHEP03(2018)179 [arXiv:1802.09535 [hep-ph]].

[10] G. S. Denicol, T. Kodama and T. Koide, J. Phys. G **37**, 094040 (2010) doi:10.1088/0954-3899/37/9/094040 [arXiv:1002.2394 [nucl-th]].

[11] H. Niemi, G. S. Denicol, P. Huovinen, E. Molnar and D. H. Rischke, Phys. Rev. Lett. **106**, 212302 (2011) doi:10.1103/PhysRevLett.106.212302 [arXiv:1101.2442 [nucl-th]].

[12] H. Niemi, G. S. Denicol, P. Huovinen, E. Molnar and D. H. Rischke, Phys. Rev. C **86**, 014909 (2012) doi:10.1103/PhysRevC.86.014909 [arXiv:1203.2452 [nucl-th]].

[13] H. Niemi, K. J. Eskola and R. Paatelainen, Phys. Rev. C **93**, no. 2, 024907 (2016) doi:10.1103/PhysRevC.93.024907 [arXiv:1505.02677 [hep-ph]].

[14] J. E. Bernhard, J. S. Moreland and S. A. Bass, Nature Phys. **15**, no. 11, 1113 (2019). doi:10.1038/s41567-019-0611-8

[15] J. Auvinen, K. J. Eskola, P. Huovinen, H. Niemi, R. Paatelainen and P. Petreczky, arXiv:2006.12499 [nucl-th].

[16] J. Y. Ollitrault, Eur. J. Phys. **29**, 275 (2008) doi:10.1088/0143-0807/29/2/010 [arXiv:0708.2433 [nucl-th]].

[17] B. H. Alver, C. Gombeaud, M. Luzum and J. Y. Ollitrault, Phys. Rev. C **82**, 034913 (2010) doi:10.1103/PhysRevC.82.034913 [arXiv:1007.5469 [nucl-th]].

[18] F. G. Gardim, J. Noronha-Hostler, M. Luzum and F. Grassi, Phys. Rev. C **91**, no. 3, 034902 (2015) doi:10.1103/PhysRevC.91.034902 [arXiv:1411.2574 [nucl-th]].

[19] D. Teaney and L. Yan, Phys. Rev. C **83**, 064904 (2011) doi:10.1103/PhysRevC.83.064904 [arXiv:1010.1876 [nucl-th]].

[20] C. E. Aguiar, Y. Hama, T. Kodama and T. Osada, Nucl. Phys. A **698**, 639 (2002) doi:10.1016/S0375-9474(01)01447-6 [hep-ph/0106266].

[21] M. Miller and R. Snellings, nucl-ex/0312008.

[22] B. Alver *et al.* [PHOBOS Collaboration], Phys. Rev. Lett. **98**, 242302 (2007) doi:10.1103/PhysRevLett.98.242302 [nucl-ex/0610037].

[23] P. Romatschke and U. Romatschke, doi:10.1017/9781108651998 arXiv:1712.05815 [nucl-th].

[24] J. F. Paquet and S. A. Bass, Phys. Rev. C **102**, no. 1, 014903 (2020) doi:10.1103/PhysRevC.102.014903

[arXiv:1912.06287 [nucl-th]].

[25] R. Baier, P. Romatschke, D. T. Son, A. O. Starinets and M. A. Stephanov, JHEP **0804**, 100 (2008) doi:10.1088/1126-6708/2008/04/100 [arXiv:0712.2451 [hep-th]].

[26] J. D. Bjorken, Phys. Rev. D **27**, 140 (1983). doi:10.1103/PhysRevD.27.140

[27] J. Vredevoogd and S. Pratt, Phys. Rev. C **79**, 044915 (2009) doi:10.1103/PhysRevC.79.044915 [arXiv:0810.4325 [nucl-th]].

[28] W. van der Schee, P. Romatschke and S. Pratt, Phys. Rev. Lett. **111**, no. 22, 222302 (2013) doi:10.1103/PhysRevLett.111.222302 [arXiv:1307.2539 [nucl-th]].

[29] H. Petersen, G. Y. Qin, S. A. Bass and B. Muller, Phys. Rev. C **82**, 041901 (2010) doi:10.1103/PhysRevC.82.041901 [arXiv:1008.0625 [nucl-th]].

[30] L. Yan, Nucl. Phys. A **967**, 89 (2017) doi:10.1016/j.nuclphysa.2017.04.022 [arXiv:1704.06643 [nucl-th]].

[31] G. Giacalone, F. G. Gardim, J. Noronha-Hostler and J. Y. Ollitrault, arXiv:2004.01765 [nucl-th].

[32] W. Broniowski, M. Chojnacki and L. Obara, Phys. Rev. C **80**, 051902 (2009) doi:10.1103/PhysRevC.80.051902 [arXiv:0907.3216 [nucl-th]].

[33] P. Bożek and W. Broniowski, Phys. Rev. C **96**, no. 1, 014904 (2017) doi:10.1103/PhysRevC.96.014904 [arXiv:1701.09105 [nucl-th]].

[34] J. Adam *et al.* [ALICE Collaboration], Phys. Rev. Lett. **116**, no. 22, 222302 (2016) doi:10.1103/PhysRevLett.116.222302 [arXiv:1512.06104 [nucl-ex]].

[35] P. Hanus, A. Mazeliauskas and K. Reygers, Phys. Rev. C **100**, no. 6, 064903 (2019) doi:10.1103/PhysRevC.100.064903 [arXiv:1908.02792 [hep-ph]].

[36] F. Gelis, G. Giacalone, P. Guerrero-Rodríguez, C. Marquet and J. Y. Ollitrault, arXiv:1907.10948 [nucl-th].

[37] B. Schenke, S. Jeon and C. Gale, Phys. Rev. C **82**, 014903 (2010) doi:10.1103/PhysRevC.82.014903 [arXiv:1004.1408 [hep-ph]].

[38] B. Schenke, S. Jeon and C. Gale, Phys. Rev. C **85**, 024901 (2012) doi:10.1103/PhysRevC.85.024901 [arXiv:1109.6289 [hep-ph]].

[39] J. F. Paquet, C. Shen, G. S. Denicol, M. Luzum, B. Schenke, S. Jeon and C. Gale, Phys. Rev. C **93**, no. 4, 044906 (2016) doi:10.1103/PhysRevC.93.044906 [arXiv:1509.06738 [hep-ph]].

[40] P. Huovinen and P. Petreczky, Nucl. Phys. A **837**, 26 (2010) doi:10.1016/j.nuclphysa.2010.02.015 [arXiv:0912.2541 [hep-ph]].

[41] A. Bazavov *et al.* [HotQCD Collaboration], Phys. Lett. B **795**, 15 (2019) doi:10.1016/j.physletb.2019.05.013 [arXiv:1812.08235 [hep-lat]].

[42] D. Teaney, Phys. Rev. C **68**, 034913 (2003) doi:10.1103/PhysRevC.68.034913 [nucl-th/0301099].

[43] P. Bozek, Phys. Rev. C **81**, 034909 (2010) doi:10.1103/PhysRevC.81.034909 [arXiv:0911.2397 [nucl-th]].

[44] J. Adam *et al.* [ALICE Collaboration], Phys. Rev. Lett. **116**, no. 13, 132302 (2016) doi:10.1103/PhysRevLett.116.132302 [arXiv:1602.01119 [nucl-ex]].

[45] D. Teaney and L. Yan, Phys. Rev. C **86**, 044908 (2012) doi:10.1103/PhysRevC.86.044908 [arXiv:1206.1905 [nucl-th]].

[46] K. Dusling and D. Teaney, Phys. Rev. C **77**, 034905 (2008) doi:10.1103/PhysRevC.77.034905 [arXiv:0710.5932 [nucl-th]].

[47] K. Dusling, G. D. Moore and D. Teaney, Phys. Rev. C **81**, 034907 (2010) doi:10.1103/PhysRevC.81.034907 [arXiv:0909.0754 [nucl-th]].

[48] J. E. Bernhard, J. S. Moreland, S. A. Bass, J. Liu and U. Heinz, Phys. Rev. C **94**, no. 2, 024907 (2016) doi:10.1103/PhysRevC.94.024907 [arXiv:1605.03954 [nucl-th]].

[49] S. S. Gubser and A. Yarom, Nucl. Phys. B **846**, 469 (2011) doi:10.1016/j.nuclphysb.2011.01.012 [arXiv:1012.1314 [hep-th]].

[50] S. Acharya *et al.* [ALICE Collaboration], Phys. Lett. B **788**, 166 (2019) doi:10.1016/j.physletb.2018.10.052 [arXiv:1805.04399 [nucl-ex]].

[51] F. G. Gardim, G. Giacalone, M. Luzum and J. Y. Ollitrault, Nature Phys. **16**, no. 6, 615 (2020) doi:10.1038/s41567-020-0846-4 [arXiv:1908.09728 [nucl-th]].

[52] S. Eremin and S. Voloshin, Phys. Rev. C **67**, 064905 (2003) doi:10.1103/PhysRevC.67.064905 [nucl-th/0302071].

[53] B. B. Back *et al.* [PHOBOS Collaboration], Phys. Rev. C **65**, 061901 (2002) doi:10.1103/PhysRevC.65.061901 [nucl-ex/0201005].

[54] J.-F. Paquet *et al.* [JETSCAPE Collaboration], arXiv:2002.05337 [nucl-th].

[55] M. Luzum and P. Romatschke, Phys. Rev. C **78**, 034915 (2008) Erratum: [Phys. Rev. C **79**, 039903 (2009)] doi:10.1103/PhysRevC.78.034915, 10.1103/PhysRevC.79.039903 [arXiv:0804.4015 [nucl-th]].

[56] E. Retinskaya, M. Luzum and J. Y. Ollitrault, Phys. Rev. C **89**, no. 1, 014902 (2014) doi:10.1103/PhysRevC.89.014902 [arXiv:1311.5339 [nucl-th]].

[57] D. Everett *et al.* [JETSCAPE Collaboration], arXiv:2010.03928 [hep-ph].